Analysis of Smith-Purcell free-electron lasers

Vinit Kumar* and Kwang-Je Kim
Advanced Photon Source, Argonne National Laboratory, Argonne, Illinois 60439, USA
(Received 19 September 2005; published 2 February 2006)

We present an analysis of the beam dynamics in a Smith-Purcell free-electron laser (FEL). In this system, an electron beam interacts resonantly with a copropagating surface electromagnetic mode near the grating surface. The surface mode arises as a singularity in the frequency dependence of the reflection matrix. Since the surface mode is confined very close to the grating surface, the interaction is significant only if the electrons are moving very close to the grating surface. The group velocity of the surface mode resonantly interacting with a low-energy electron beam is in the direction opposite to the electron beam. The Smith-Purcell FEL is therefore a backward wave oscillator in which, if the beam current exceeds a certain threshold known as start current, the optical intensity grows to saturation even if no mirrors are employed for feedback. We derive the coupled Maxwell-Lorentz equations for describing the interaction between the surface mode and the electron beam, starting from the slowly varying approximation and the singularity in the reflection matrix. In the linear regime, we derive an analytic expression for the start current and calculate the growth rate of optical power in time. The analysis is extended to the nonlinear regime by performing a one-dimensional time-dependent numerical simulation. Results of our numerical calculation compare well with the analytic calculation in the linear regime and show saturation behavior in the nonlinear regime. We find that a significant amount of power grows in the surface mode due to this interaction. Several ways to outcouple this power to freely propagating modes are discussed.

DOI: 10.1103/PhysRevE.73.026501 PACS number(s): 41.60.Cr, 42.79.Dj, 52.59.Px

I. INTRODUCTION

An electron traveling close and parallel to a metallic reflection grating, with grating rulings perpendicular to the electron motion, gives off polarized electromagnetic radiation [1–3] having the wavelength given by

$$\lambda = \frac{\lambda_g}{|m|\beta}(1 - \vec{\beta}\cdot\vec{n}), \tag{1}$$

where λ_g is the grating period, $\vec{\beta}\equiv\vec{v}/c$ is the electron velocity in the unit of speed of light c, $\vec{n}$ is the unit vector along the emission direction, and m is the spectral order. This radiation was first observed by Smith and Purcell in 1953 [3], and since then has been known by their name. Smith-Purcell (SP) radiation has been studied for more than 50 years, and many theoretical and experimental investigations have been made since then [4–32]. Studies have been performed on generating SP radiation using low-energy (~35 keV) electrons from scanning electron microscopes [23,28,31] and electron beam welding machines [24], as well as high-energy beam (up to 855 MeV) from electron accelerators [30]. One can obtain THz radiation with a low-energy electron beam if the grating period is around 100–200 μm. Recently, the idea of using the low-energy and good-quality electron beam from a scanning electron microscope (SEM) to make a THz SP free-electron laser (FEL) by retrofitting a grating into the SEM has been proposed and explored experimentally [28,31]. A tunable, coherent THz source based on SP radiation will be attractive due to its compact size.

Smith-Purcell radiation arises due to the periodic motion of the induced electrostatic image charge. A rigorous theoretical analysis can be performed based on the scattering of the incident evanescent wave [4]. In this approach, which we follow in this paper, the electromagnetic field due to a uniformly moving charged particle is expressed as superposition of plane waves of different spatial frequencies having the phase velocity equal to the particle velocity. These waves, which are nonradiative evanescent waves, decay exponentially away from the electron beam and are essentially the Fourier components of the Coulomb field transformed from electron's rest frame to the laboratory frame.

When incident on a grating, the waves are reflected at various spectral orders due to the periodicity of the grating. Knowing the amplitude reflectivity e_{m0} (which is the ratio of the amplitude of the mth order reflected wave to the zeroth-order incident wave), the radiation amplitude of outgoing waves at any spectral order can be calculated for the given frequency. For some of these spectral orders, the propagation vectors are real. These waves can propagate electromagnetic energy away from the grating and are called "propagating waves." These are far-field terms in the total electromagnetic field. For the remaining spectral orders, the component of the propagation vector normal to the grating is imaginary, and hence they cannot propagate electromagnetic energy away from the grating. These are called "evanescent waves" or "surface waves" for which the electromagnetic energy is confined to the grating. These are near-field terms in the total electromagnetic field.

Evaluation of the reflection matrix elements of a grating is an involved problem and has been studied for more than 100 years, beginning with the work of Lord Rayleigh [33]. It was only in the latter half of the 20th century that numerical

*Permanent address: G-20, ADL Building, Raja Ramanna Centre for Advanced Technology, Indore–452013, India.

computation of these matrix elements was started [34]. Matrix elements e_{m0} were first evaluated for the outgoing propagating modes by Van den berg [6–8]. The SP radiation spectrum for spontaneous emission calculated by this method was later found to agree well with the experimental data [23].

The beam-grating system can, under certain circumstances, act as gain medium, and hence the device can be operated as a laser, which will be referred as a SP free-electron laser (FEL). Early attempts to generate coherent radiation using the SP effect were made by Rusin and Bogmolov [16], and they named their device "Orotron." Later Mizuno *et al.* constructed a similar device, which they named "Ledatron" [19]. These devices used an open resonator and generated power output in the frequency range 60–90 GHz but were not extended beyond this range. Wachtell [9] performed a theoretical analysis of SP-FEL using a different resonator configuration and proposed that the operation of the device could be extended to the infrared region. A more general analysis of SP-FEL was developed by Schachter and Ron [10] in the linear regime. They developed the theory in terms of reflection matrix elements but used some approximation to evaluate these elements and found a cubic equation for the growth rate that is typical of a traveling wave amplifier (TWA)-type interaction. Kim and Song [14] used the Maxwell-Klimontovich approach [35], solved the initial value problem for the sheet-beam case, and found a quadratic equation for the growth rate. Their theory was also in terms of reflection matrix elements, and they used the approximation that the scattering matrix e_{00} is smooth. A quadratic equation for the growth rate was remarkable because it meant an interaction different from the TWA type. More recently, Andrews and Brau [15] performed an analysis for the infinite electron beam, treating it as a moving dielectric, and solved the Maxwell equations for the rectangular grating case and obtained a cubic equation for the growth rate. Taken at face value, these three analyses do not agree well with each other, as pointed out in Ref. [15]. Here, we present a more general analysis of SP-FELs by extending the Kim and Song approach and evaluating the reflection matrix elements e_{mn} as a function of frequency. Our calculation of e_{mn} is based on the method used by Van den berg [8,36], and we extend it to the case of waves with slowly varying amplitude. This analysis gives us the growth rate in space, as a function of frequency for SP-FELs. The growth rate spectrum reveals some interesting physics of SP-FELs, which we discuss in this paper. We show that a proper evaluation of singularities of the reflection matrix element removes the inconsistency among the three analyses mentioned above.

The singularity in the reflection matrix means that the grating supports a surface electromagnetic mode. The gain mechanism in the SP-FEL comes from the interaction of the electron beam with the copropagating surface wave. As first pointed out by Andrews and Brau [15], for the low-energy electron beam, the group velocity of the surface mode is in the direction opposite to that of the copropagating electron beam. The SP-FEL therefore works like a backward wave oscillator (BWO) and is fundamentally different from conventional FELs in many aspects. First, due to the negative group velocity, there is a built-in feedback mechanism, and the device can act as an oscillator without any external feedback. Second, there exists a threshold current, called the start current, such that the power grows exponentially in time only when the beam current is higher than the start current. For an ideal monoenergetic electron beam, there is no such threshold current for conventional FELs. We study these aspects of SP-FEL in detail in this paper.

We should mention here that although SP-FEL in the parameter regime we studied in this paper works as a BWO, it can work as a TWA in other parameter regimes, such as with higher electron energy. The group velocity of the relevant surface wave in that case is in the direction of the electron beam. Analysis of an SP-FEL based on TWA interaction, either as an oscillator with feedback, or as a high-gain single-pass amplifier, can be developed similary as in a usual undulator-based FEL.

Previous analyses of SP-FELs have been mostly in the linear regime. In order to obtain a complete picture of the device and to understand the efficiency, the growth of power, and bunching, etc., it is essential to understand the saturation behavior, which demands a nonlinear analysis of the problem. There have been earlier attempts to do the analysis in the nonlinear regime [37,38], but these analyses are not completely self-consistent in that the Maxwell equation is not solved as coupled to electron dynamics; instead, a certain mode structure for the electromagnetic field is assumed. In this paper, we present a nonlinear self-consistent analysis of SP-FELs assuming a sheet electron beam. We have developed a one-dimensional time-dependent computer code for SP-FELs driven by a sheet electron beam and taking the BWO-type interaction into account. We used our computer code to study the detailed behavior of SP-FELs and present the results in this paper.

The paper is organized as follows. In the next section, we present the basic analysis using the slowly varying approximation and present our results in terms of reflection matrix elements. In Sec. III we discuss the results of numerical evaluation of reflection matrix element e_{00} and show that it becomes singular at a certain resonant frequency due to the existence of the surface mode supported by the grating having a phase velocity equal to the electron velocity. We study the behavior around this singularity and the frequency dependence of the growth rate. Next, we set up one-dimensional time-dependent coupled Maxwell-Lorentz equations to analyze the nonlinear behavior in Sec. IV. Analytic solutions of these equations in the linear regime are discussed in Sec. V where we derive an analytic expression for the start current and calculate the growth rate of power in time. In Sec. VI we discuss the results of our simulations and explicitly show that the electron beam becomes bunched due to the BWO-type interaction. We then discuss various ways of outcoupling the radiation energy in the SP-FEL system in Sec. VII. Finally, we present some discussions and conclude in Sec. VIII.

II. BASIC ANALYSIS UNDER THE SLOWLY VARYING APPROXIMATION

Let us begin the analysis by writing down the electromagnetic field due to a continuous electron beam. Figure 1 shows

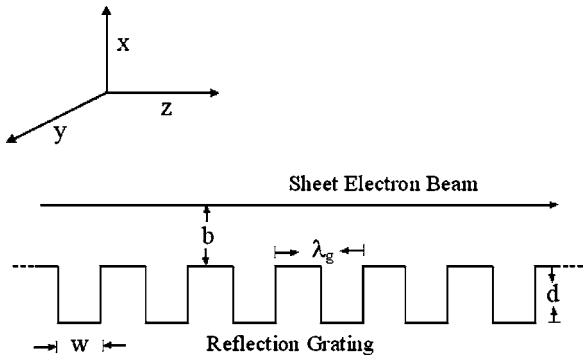

FIG. 1. Schematic of an SP-FEL using a sheet electron beam. The sheet electron beam is in the plane $x=0$.

a schematic of the SP-FEL setup. We assume the system to be translationally invariant in the y direction. For simplicity, we consider a sheet beam and later present the results for the more general case. The electron beam travels with a speed v along the z axis, at a height b above the grating having grooves of depth d, width w, and period λ_g. The expression for the z component of the current density is given by

$$J_z(x,z,t) = \frac{q}{\Delta y}\delta(x)\sum_i \delta[t - t_i(z)], \tag{2}$$

where q is electron's charge, t_i is the time at which the ith particle arrives at z, and Δy is the thickness of the sheet beam. Note that the summation is over all the electrons. The Fourier transform of the current density is then given by

$$J_z(x,z,\omega) = \int_{-\infty}^{+\infty} J_z(x,z,t)e^{i\omega t}dt = \delta(x)K(z,\omega)e^{ik_0 z}, \tag{3}$$

where

$$K(z,\omega) = \frac{q}{\Delta y}\sum_i e^{i\omega\xi_i}. \tag{4}$$

Here, $k_0=\omega/c\beta$ and $\xi_i=t_i-z/v$. If we neglect the interaction with the electromagnetic field, the electrons will be moving with uniform velocity and $K(z,\omega)$ will then be independent of z. Considering the interaction with the electromagnetic field, it is a function of z. As usual, we will assume the z dependence to be slow. In the linear regime, we assume a solution for $K(z,\omega)$ of the type $K_0(\omega)e^{\mu z}$ and look for possible solutions for μ. If the real part of μ is positive, it would mean exponential growth of $K(z,\omega)$, implying enhanced bunching at the particular frequency.

Solving the Maxwell equations with the above current density, one finds the following expression for the electromagnetic field due to the electron beam, which acts as an incident field on the grating

$$H_y^I(x,z,\omega) = \frac{1}{2}\varepsilon(x)K_0(\omega)\exp[i\alpha_0 z - \varepsilon(x)\Gamma_0 x], \tag{5}$$

where $\alpha_0=k_0-i\mu$, $\Gamma_0=(\alpha_0^2-\omega^2/c^2)^{1/2}$, $\varepsilon(x)=-1$ for $x<0$, and $\varepsilon(x)=1$ for $x>0$. Note that $x=0$ is the location of the sheet beam. The electromagnetic field has H polarization, which means $H_x^I=H_z^I=E_y^I=0$. The E_z^I can be obtained in terms of H_y^I by $E_z^I=(i/\epsilon_0\omega)(\partial H_y^I/\partial x - J_z)$. Note that this electromagnetic field has the form of a plane wave, has the phase velocity the same as the electron beam, and decays exponentially away from the beam; hence it does not radiate. Let us call it the zeroth-order wave. We define $\lambda=2\pi c/\omega$ as the free-space wavelength.

Next, let us consider the effect due to the grating. Owing to the periodicity of the grating and using the Floquet-Bloch expansion, the incident and reflected plane waves can be expressed as $\Sigma A_n^I \exp(i\alpha_n z - ip_n x)$ and $\Sigma A_n^R \exp(i\alpha_n z + ip_n x)$, respectively, where n is the spectral order, and the summation is implied over all n from $-\infty$ to $+\infty$. Here, $\alpha_n=\alpha_0 - nk_g$, where $k_g=(2\pi/\lambda_g)$, $p_n=i\Gamma_n=(\omega^2/c^2-\alpha_n^2)^{1/2}$, and the sign of the square root is chosen such that $[\mathrm{Re}(p_n)+\mathrm{Im}(p_n)]\geqslant 0$, which is essentially the outgoing wave condition [34]. A given nth order wave is propagating if p_n is real and is evanescent if Γ_n is real. Note that all the modes with $n\leqslant 0$ are evanescent, and some of the modes having $n>0$ may be propagating depending on the grating period and the frequency. The reflection matrix e_{mn} of the grating couples the nth-order incident wave to the mth-order outgoing wave at the grating surface, i.e., $A_m^R=\Sigma e_{mn}A_n^I$. In our case, to start with, we have only the zeroth-order incident wave with known amplitude given by Eq. (5). Knowing the various e_{m0}, Van den berg [6–8] calculated the amplitude of reflected waves for propagating orders, which is observed as spontaneous SP radiation.

If the electron beam current is sufficiently high, the electrons interact with the field, and the current density will be modified. Out of all the spectral orders, the electron beam interacts most effectively with the zeroth-order wave since only the zeroth-order wave has a phase velocity the same as the beam velocity. The higher-order waves produce higher-order modulation in the current desnsity $K(z,\omega)$, but the interaction is feeble since the phase velocity of the higher-order wave is not matched with the electron velocity. The higher-order modulation in the current density could give rise to higher-order incident waves, which we do not consider here. The electron beam therefore effectively experiences the field only due to the zeroth-order incident and reflected waves. However, we need to include higher-orders contained in the surface mode in order to satisfy the boundary conditions. The electromagnetic field of the zeroth-order reflected wave is given by

$$H_y^R(x=0,z,\omega) = -\frac{1}{2}K_0(\omega)e_{00}\exp(-2\Gamma_0 b)\exp(i\alpha_0 z). \tag{6}$$

The total electric field experienced by the electrons is obtained by adding the contribution due to incident and reflected zeroth-order waves at $x=0$,

$$E_z(x=0,z,\omega) = \frac{i\Gamma_0}{2\epsilon_0\omega}(e_{00}e^{-2\Gamma_0 b}-1)K_0(\omega)e^{i\alpha_0 z}. \tag{7}$$

Next, we discuss the beam dynamics. We assume that electrons experience only the longitudinal force due to the above electric field and neglect transverse motion due to E_x. Let $f(\xi,\eta,z)$ be the electron distribution function

$$f(\xi,\eta,z)=\frac{q}{I}\sum_i \delta(\xi-\xi_i)\delta(\eta-\eta_i), \tag{8}$$

where I is the beam current, $\eta=\delta\gamma/\gamma$ is the relative deviation in electron's energy from its average value, and γ is electron's energy in units of rest mass energy mc^2. We can express the above distribution as the sum of two parts,

$$f(\xi,\eta,z)=\bar{f}_0(\eta)+\delta f(\xi,\eta,z), \tag{9}$$

where $\bar{f}_0$ is the initial smoothened, unbunched distribution function, and δf is the perturbation. Note that $\bar{f}_0(\eta)$ is the input energy distribution of the electron beam, and its normalization condition is $\int\bar{f}_0(\eta)d\eta=1$. In order to study the evolution from shot noise, one has to take into account the discreteness of electrons. Since we are studying the growth rate of the eigenmode supported by the SP-FEL system, here we will ignore the discreteness of electrons and treat δf as a smooth function. The surface current density $K(\omega,z)$ can be expressed in terms of the Fourier transform of the distribution function as

$$K(\omega,z)=\left(\frac{I}{\Delta y}\right)\int_{-\infty}^{+\infty}\delta f_\omega(\eta,z)d\eta, \tag{10}$$

where

$$\delta f_\omega(\eta,z)=\int_{-\infty}^{+\infty}\delta f(\xi,\eta,z)\exp(i\omega\xi)d\xi. \tag{11}$$

The evolution of the smoothened distribution function is given by the Vlasov equation, which takes the following form:

$$\frac{\partial\delta f}{\partial z}+\dot{\xi}\frac{\partial\delta f}{\partial\xi}+\dot{\eta}\frac{\partial\delta f}{\partial z}=0, \tag{12}$$

where "·" is used for the total derivative with respect to z, and the expressions for $\dot{\xi}$ and $\dot{\eta}$ are given by the following equations of motion

$$\dot{\xi}=-\frac{\eta}{c\beta^3\gamma^2},\quad \dot{\eta}=\frac{q}{\gamma mc^2}e^{-ik_0z}E(\xi,z), \tag{13}$$

where

$$E(\xi,z)=\frac{1}{2\pi}\int_{-\infty}^{+\infty}E_z(x=0,z,\omega)e^{-i\omega\xi}d\omega. \tag{14}$$

Substituting Eq. (13) in Eq. (12) and then taking the Fourier transform, we obtain an equation for δf_ω. Since we are looking for an exponential solution of the type $\delta f_\omega(\eta,z)=\delta f_\omega(\eta,0)e^{\mu z}$, we solve this equation for δf_ω and substitute the solution into Eq. (10) to obtain the following expression for the induced surface current density in terms of electric field:

$$K(\omega,z)e^{ik_0z}=K_0(\omega)e^{i\alpha_0z}=-\frac{IqE_z}{\Delta y\,\gamma mc^2}T(\mu), \tag{15}$$

where $T(\mu)$ is given by

$$T(\mu)=\int d\eta\frac{\partial\bar{f}_0(\eta)}{\partial\eta}\frac{1}{\mu+\dfrac{i\omega\eta}{c\beta^3\gamma^2}}. \tag{16}$$

Putting Eq. (15) in Eq. (7) and assuming monoenergetic initial distribution, i.e., $\bar{f}_0(\eta)=\delta(\eta)$, we obtain the following equation for μ:

$$\mu^2=\frac{1}{\gamma^3\beta^3}\frac{2\pi\Gamma_0}{\Delta y}\frac{I}{I_A}(e_{00}e^{-2\Gamma_0b}-1), \tag{17}$$

where $I_A=4\pi\epsilon_0mc^3/e=17.04$ kA is the Alfvén current. Note that the above expression for the growth rate is same as obtained in Ref. [14] except that the second term in the small bracket, which is the contribution due to space charge, was omitted there.

We have performed the above analysis for the case of a uniform-density electron beam of finite thickness Δx in the x direction and derived the following equation, which needs to be solved to obtain the growth rate:

$$\frac{1}{e_{00}}=\frac{-(\Upsilon_0^2+\Gamma_0^2)\sin(\Upsilon_0\Delta x)\exp(-2\Gamma_0b)}{2\Gamma_0\Upsilon_0\cos(\Upsilon_0\Delta x)+(\Gamma_0^2-\Upsilon_0^2)\sin(\Upsilon_0\Delta x)}, \tag{18}$$

where

$$\Upsilon_0=i\Gamma_0\left(1-i\frac{4\pi c}{\omega\gamma\Delta y\Delta x}\frac{I}{I_A}T(\mu)\right)^{1/2}. \tag{19}$$

Note that the above equation, for the monoenergetic case, is exactly the same as that obtained by Schachter and Ron [10], and, in the limit $\Delta x\to 0$, we obtain Eq. (17) back. By taking the limits $\Delta x\to\infty$ and $I/\Delta x\to I_0$, we obtain the infinite beam case studied by Andrews and Brau [15].

III. SINGULARITY IN THE REFLECTION MATRIX AND SURFACE MODE

The evaluation of the reflection matrix for grating of different profiles has been a subject of extensive study [34,36]. For rectangular gratings, Van den berg has used the modal expansion method, which is relatively faster [8]. In Van den berg's calculations, the outgoing waves are propagating waves, whereas, for the present calculation, we need to perform the calculation where the outgoing wave is also the zeroth-order evanescent wave. Details of our calculation of e_{00} for rectangular grating can be found elsewhere [39]. For our calculation, we have used the parameters corresponding to the Dartmouth experiment by Urata *et al.* [28], which are given in Table I.

Figure 2 shows the plot of e_{00} versus wavelength. We have used the modal method for this calculation, and we have included a sufficient number of modes such that our calculation converges to an accuracy of better than 1%. Several important points are revealed by this plot. First of all, there is a singularity at 690 μm preceded by a zero at 675.2 μm. A singularity in e_{00} means that the grating supports the zeroth-order outgoing evanescent wave on its own, i.e., without any incident wave, by the self-consistent current on the grating surface. This would imply that e_{0m} will have,

TABLE I. Parameters of the SP-FEL used in the calculation

Grating period (λ_g)	173 μm
Groove width (w)	62 μm
Groove depth (d)	100 μm
Electron energy	35 keV
Beam height from grating top surface (b)	10 μm
Beam surface current density (I)	50 A/m

in general, singularity for *any* spectral order m. The reciprocity relation [34] implies that $p_m e_{m0} = \Gamma_0 e_{0m}$. Therefore, e_{m0} will also have singularity for all spectral orders m included in the Fourier-Bloch expansion. Thus, whenever a singularity exists in e_{00}, the grating supports all spectral-order outgoing modes at that frequency, which are included in the Fourier-Bloch expansion. If any of these modes is propagating, that would imply that energy will flow out of the grating without any source, violating the energy conservation. Hence, we conclude that the singularity in e_{00} should occur only at those frequencies at which none of the outgoing modes is propagating. That is indeed the case at 690 μm; none of the spectral modes at this wavelength are propagating. Actually, for any grating, there is a threshold wavelength $\lambda_{th} = (\lambda_g/\beta)(1+\beta)$ above which all spectral orders are evanescent. For our parameters, $\lambda_{th} = 667.3$ μm. In our case, both zero and pole occur at wavelengths longer than λ_{th}. The zero and pole for a metallic grating including the finite conductivity was discussed by Neviere [40] for propagating modes.

When the groove depth tends to zero, we should obtain $e_{00} = 1$ for all wavelengths. That indeed happens. The separation between the pole and zero wavelengths reduces as we reduce the groove depth and vanishes when the groove depth tends to zero; then we obtain $e_{00} = 1$.

Now we come back to Eq. (17) and discuss the growth rate. The straightforward substitution of e_{00} in Eq. (9) would mean that, at the singularity, the growth rate should tend to infinity, which does not make sense. We resolve this by realizing that e_{00} should actually be a function of μ also. By

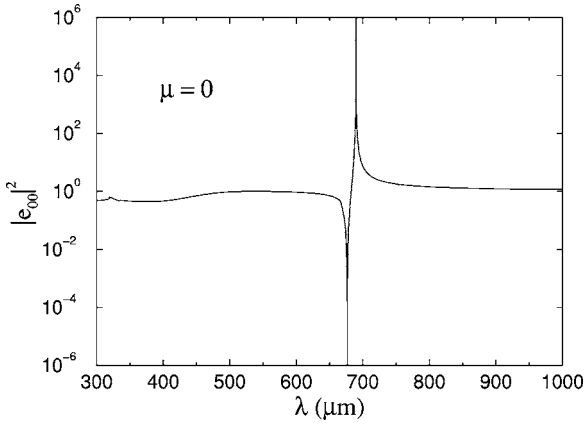

FIG. 2. Plot of e_{00} as a function of free-space wavelength of the zeroth-order evanescent wave for $\lambda_g = 173$ μm, $d = 100$ μm, $w = 62$ μm, and $\beta = 0.35$. Note that e_{00} has a zero at 675.2 μm followed by a singularity at 690 μm.

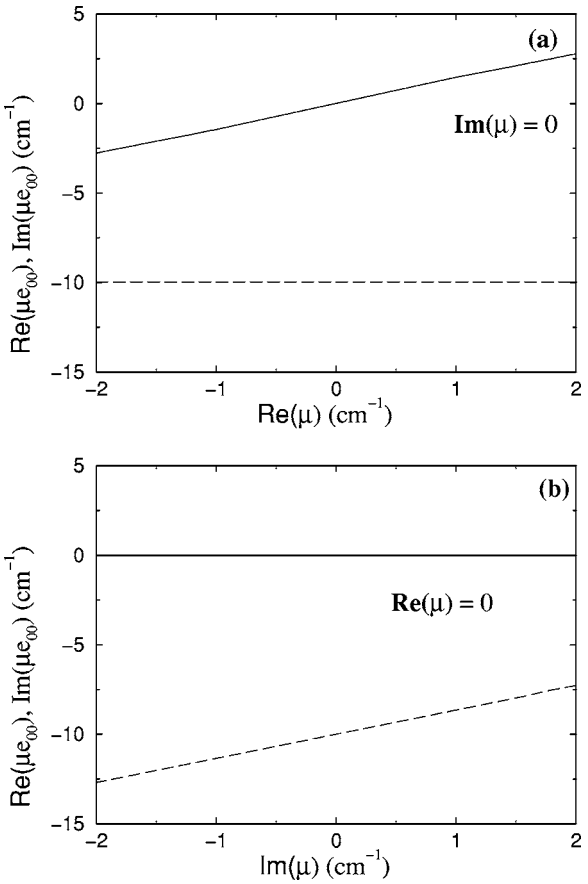

FIG. 3. Plots of real (solid) and imaginary (dashed) parts of μe_{00} as a function of the real (a) and imaginary (b) parts of the growth parameter μ around the singularity, i.e., at 690 μm. The grating parameters are the same as in Fig. 2. From these plots, it is clear that e_{00} can be parametrized as $-i\chi/\mu + \chi_1$, and we get $\chi = 10$ per cm and $\chi_1 = 1.35$ from these plots.

making the wave vector complex, we perform the calculation of e_{00} as a function of growth rate. In this calculation, we have included more higher-order components such that our calculation converges to an accuracy of better than 0.1%. We first determine the nature of singularity at $\mu = 0$. We assume that the singularity is a pole of mth order, where m is to be determined. The order m of the pole at $\mu = 0$ is obtained as the smallest integer such that $\mu^m e_{00}$ becomes a nonsingular function around $\mu = 0$. We find that around $\mu = 0$, μe_{00} has no singularity and is an analytic function of μ as shown in Fig. 3. This implies that $m = 1$ and hence, the singularity of e_{00} is a simple pole. Also, we find from Fig. 3 that e_{00} can be expressed as $-i\chi/\mu + \chi_1$, where we have kept only the first two terms in the Laurent series. From Fig. 3, we find $\chi = 10$ per cm, and $\chi_1 = 1.35$. Substituting this μ dependence of e_{00} in Eq. (17), we find that the growth rate equation becomes cubic near the singularity as obtained by other authors [10,15]. Our calculation crucially depends on the accurate location of the singularity. In order to achieve this in an iterative manner, we have first determined the approximate location of the singularity as in Fig. 2, and then we went on narrowing the window around the approximate location. Note that one can determine the value of χ and χ_1 using any

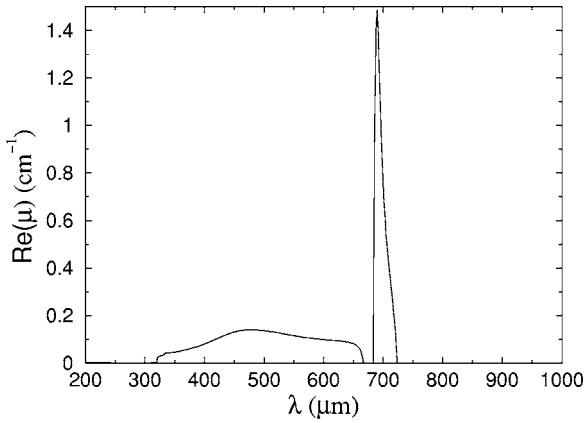

FIG. 4. Growth rate plotted as a function of wavelength for $I/\Delta y=50$ A/m and $b=10$ μm. Grating parameters are again the same as in Fig. 2. Note that there are two regions. Region I spans from 320 μm to 667 μm, where some of the spectral orders are radiative. Here, the peak growth rate is 0.15 per cm at 478 μm. Region II is relatively sharper and peaked at 690 μm, and the peak growth rate here is 1.5 per cm. Note that all the spectral orders in region II are evanescent.

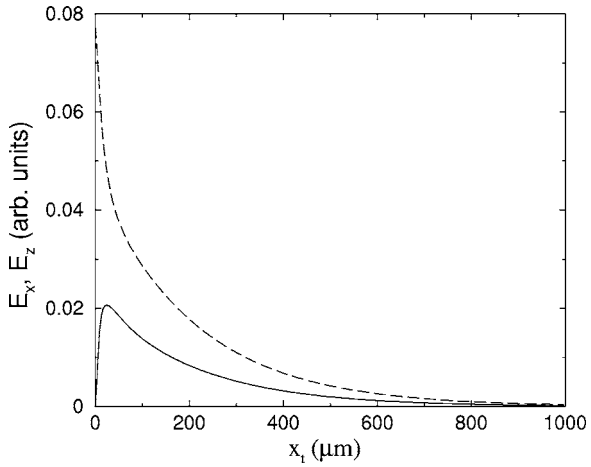

FIG. 5. Plot of the longitudinal electric field E_z (solid line) and the transverse electric field E_x (dashed line) of the surface mode supported by the grating, as a function of the distance x_t from the top surface of the grating.

one of the graphs in Fig. 3, either Fig. 3(a), or Fig. 3(b). If the location of the singularity is obtained accurately, the value of χ and χ_1 obtained separately from these two graphs should be equal, which is indeed the case in our calculation.

This behavior changes if we are significantly away from the singularity. We find that e_{00} has extremely weak dependence on μ. In that case, the growth rate equation is quadratic as obtained by Kim and Song [14]. We emphasize that it is indeed this type of interaction, different from the usual FEL/TWA-type interaction, which gives a cubic equation for the growth rate.

Hence, the correct way to evaluate the growth rate at any given frequency is to take the μ dependence of e_{00} in Eq. (9) and solve this equation by an iterative method until the desired accuracy is achieved. In our calculation, we set an accuracy of better than 1%. Figure 4 shows the plot of growth rate as a function of wavelength obtained using this method. In this figure, we set $I/\Delta y=50$ A/m and $b=10$ μm to mimic the Dartmouth experiment [28] in which a circular beam of radius 10 μm and current 1 mA was employed. We clearly see that there are two regimes. The first regime is a broad band and covers the range from 320 μm to 667 μm. This is followed by the second regime, which starts at 686 μm and decays relatively sharply. In the first regime, which is below λ_{th}, propagating modes are allowed and the radiation can be observed, but not so in the second regime. The gain in the first regime is low, the peak is at 478 μm where the amplitude growth rate is 0.15 per cm. In the second regime, no radiative mode is allowed, and the gain is peaked at 690 μm, i.e., at the location of the pole of e_{00}. The peak growth rate is calculated to be 1.5 per cm. We have also carried out these calculations for the infinite-beam case, and our results (both the wavelength and the gain) agree with the results obtained by Andrews and Brau [15].

Next, we discuss the surface mode supported by the grating. For a given phase velocity βc of the zeroth-order incident evanescent wave, the reflection matrix element e_{00} becomes singular at a certain frequency ω_s. This means that, at frequency ω_s, the grating supports a surface mode consisting of a zeroth-order evanescent component having $k_s=\omega_s/c\beta$ and the higher-order components with suitable amplitude in order to satisfy the boundary condition at the grating surface. In the remaining part of the paper, we will drop the subscript in ω_s and use ω as the frequency of the surface mode.

Figure 5 shows the electric field profile of this surface mode at $z=0$ for our parameters. In our calculation, we find that, overall, the $n=1$ component has the strongest contribution to the total field. However, near the grating surface, i.e., at $x_t=0$, the contributions of other components become very important; this is required in order that the boundary condition is satisfied on the grating surface. Since the $n=1$ mode has its phase velocity in the backward direction, we expect that the net energy flows backward. This is consistent with Fig. 6, which shows the dispersion relation of this surface mode. In our analysis, We find that, when the electron beam energy is low ($\sim$35 keV), the group velocity $d\omega/dk$ is negative. When the phase velocity equals the velocity of a 35-keV electron beam, the group velocity is in the direction opposite to the electron beam and 0.53 times the speed of light in magnitude. To summarize, the electron beam interacts with the zeroth-order component of the surface mode with a phase velocity matched with the beam, but the energy given up by the electron to the surface mode is flowing backward.

The dispersion curve that we have obtained is the same as the one obtained by Andrews and Brau [15]. This is because we both neglect the electron beam in computing the dispersion curve for the surface mode. Our only difference is in the method of eigenmode determination; they use the eigenmodes of the groove as the basis set in their analysis whereas we use the eigenmodes of the free space above the grating as the basis set in our analysis. These two approaches give similar result.

The fact that the group velocity is negative, first observed in Ref. [15], changes the character of the power build-up in a

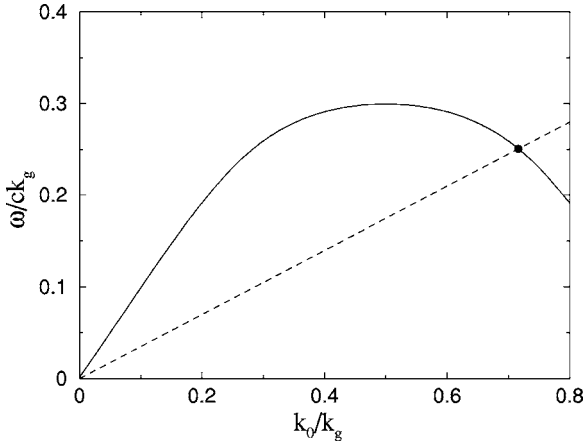

FIG. 6. The solid line shows the dispersion curve of the surface mode supported by the grating for the parameters mentioned earlier. The dashed line is the Doppler line for the beam. At the intersection point, the group velocity v_g is negative and its value is $0.54c$, as obtained from this plot.

Smith-Purcell system from the conventional FELs. In conventional FELs, the optical power grows as the radiation beam travels along the electron beam direction. If the single-pass gain is not high, an external mirror system reflects back the optical beam to the entrance of the interaction regime so that the power can build up to saturation after many round trips. The mirror system is not necessary only if the single-pass gain is very high, as in the case of recent x-ray FEL projects. When the group velocity is in the opposite direction, as in the Smith-Purcell system under discussion at $\lambda = 690\ \mu$m, the optical power in the interaction region can continually build up without the use of an external mirror system. This is because the backward flow of energy modifies the dynamics of the incoming electrons at the entrance. These electrons, as they move down the grating, again give off energy to the surface mode, which flows backward and again interacts with the incoming electrons, and the process continues. Such a system is known as a backward wave oscillator (BWO) in microwave engineering [41].

IV. THE COUPLED MAXWELL-LORENTZ EQUATIONS FOR A BWO

In this section, we will set up the Maxwell-Lorentz equation for the interaction of the electron beam with the electromagnetic wave supported by the grating. This is similar to what is done for the case of conventional FELs, and it has turned out to be very useful for the detailed analysis there [42]. Such an analysis was later developed for a BWO [43,44].

Let us start by writing down the expression for the amplitude E_z of the axial electric field experienced by the sheet electron beam. The surface current density can be written as $(I/\Delta y)\langle e^{-i\psi}\rangle e^{i(k_0 z-\omega t)}$+c.c., where $\langle \ldots \rangle$ implies averaging over the number of electrons distributed over one wavelength of a zeroth-order evanescent wave. Note that $\omega = ck$ here refers to the frequency of the surface mode and $k_0 = k/\beta$. Using Eq. (7), we obtain the following expression for the amplitude of the longitudinal electric field:

$$E_z = \frac{iIZ_0}{2\beta\gamma\Delta y}\left(\frac{-i\chi}{\mu}e^{-2\Gamma_0 b} + \chi_1 e^{-2\Gamma_0 b} - 1\right)\langle e^{-i\psi}\rangle. \quad (20)$$

where the electron phase $\psi = k_0 z - \omega t$, $Z_0 = 1/\epsilon_0 c = 377\ \Omega$ is the chracteristic impedence of free space, and ϵ_0 is the permittivity of free space. Note that the total longitudinal electric field is given by $E_z e^{(ik_0 z-\omega t)}$+c.c. The above expression has two parts. The first part corresponding to the first term is the outgoing evanescent mode, which is a component of surface mode. The remaining terms are independent of growth rate and are identified as space-charge terms. Let us denote the surface-mode component as E and the space-charge component as E_{sc}. In the expression for E, we can replace μ with the operator d/dz and obtain the steady-state differential equation for E. Incorporating the group velocity, this equation is further generalized to the following time-dependent differential equation for E:

$$\frac{\partial E}{\partial z} - \frac{1}{v_g}\frac{\partial E}{\partial t} = \frac{IZ_0\chi}{2\beta\gamma\Delta y}e^{-2\Gamma_0 b}\langle e^{-i\psi}\rangle. \quad (21)$$

The expression for the space charge field is given by

$$E_{sc} = \frac{-iIZ_0}{2\beta\gamma\Delta y}(1 - \chi_1 e^{-2\Gamma_0 b})\langle e^{-i\psi}\rangle. \quad (22)$$

Here v_g is the group velocity in the backward direction, so it is a positive quantity for our Smith-Purcell system. Note that Eq. (21) describes only the zeroth-order evanescent component of the surface mode. The amplitudes of higher-order spectral components are completely determined in terms of the amplitude of the zeroth-order component uniquely, such that the boundary condition at the grating is satisfied. Equations (21) and (22) are the Maxwell equations that we will be using in our analysis.

Next, we discuss the equations for the electron dynamics. Assuming the electron motion to be one dimensional, we describe the longitudinal dynamics of the ith electron in terms of phase ψ_i and energy (in units of rest mass energy) γ_i. We can derive the following equation of motion for the electron in the presence of a surface wave and the space-charge field:

$$\frac{\partial \gamma_i}{\partial t} + v\frac{\partial \gamma_i}{\partial z} = \frac{ev}{mc^2}(E + E_{sc})e^{i\psi_i} + \text{c.c.}, \quad (23)$$

$$\frac{\partial \psi_i}{\partial t} + v\frac{\partial \psi_i}{\partial z} = \frac{\omega}{\beta^2\gamma^2}\frac{(\gamma_i - \gamma_p)}{\gamma_p}. \quad (24)$$

Here, the electron velocity v is close to the phase velocity v_p of the zeroth-order evanescent component of the surface mode. Equations (21)–(24) are the full set of coupled Maxwell-Lorentz equations, which govern the behavior of the sheet-beam SP-FEL with the given boundary conditions. These equations can be solved numerically. Before proceeding with the numerical solution, we define the following dimensionless variables:

$$\zeta = z/L, \quad (25)$$

$$\tau = \left(t - \frac{z}{v_p}\right)\left(\frac{1}{v_p} + \frac{1}{v_g}\right)^{-1}\frac{1}{L}, \tag{26}$$

$$\eta_i = \frac{k_0 L}{\beta^2\gamma^3}(\gamma_i - \gamma_p), \tag{27}$$

$$\mathcal{E} = \frac{4\pi}{I_A Z_0}\frac{k_0 L^2}{\beta^2\gamma^3}E, \tag{28}$$

$$\mathcal{E}_{sc} = \frac{4\pi}{I_A Z_0}\frac{k_0 L^2}{\beta^2\gamma^3}E_{sc}, \tag{29}$$

$$\mathcal{J} = 2\pi\frac{I}{I_A}\frac{\chi}{\Delta y}\frac{k_0 L^3}{\beta^3\gamma^4}e^{-2\Gamma_0 b}. \tag{30}$$

Here, L is the total length of the grating, and ζ is the dimensionless distance along the grating, which varies from 0 to 1. The dimensionless time variable τ is offset from the real time t by z/v_p and then normalized. The dimensionless electric field amplitudes for the zeroth-order component of the surface wave and the space-charge field are given by $\mathcal{E}$ and $\mathcal{E}_{sc}$, respectively. The dimensionless beam current is given by $\mathcal{J}$, and η_i is the normalized energy-detuning of the ith electron. In terms of these dimensionless variables, the coupled Maxwell-Lorentz equations take the following form:

$$\frac{\partial\mathcal{E}}{\partial\tau} - \frac{\partial\mathcal{E}}{\partial\zeta} = -\mathcal{J}\langle e^{-i\psi}\rangle, \tag{31}$$

$$\frac{\partial\eta_i}{\partial\zeta} = (\mathcal{E} + \mathcal{E}_{sc})e^{i\psi_i} + \text{c.c.}, \tag{32}$$

$$\frac{\partial\psi_i}{\partial\zeta} = \eta_i, \tag{33}$$

$$\mathcal{E}_s = iQ\langle e^{-i\psi}\rangle, \tag{34}$$

where $Q=(\mathcal{J}/\chi L)(\chi_1 - e^{2\Gamma_0 b})$. As we show in Appendix A, using the conservation of energy, we get the following expression for the power in the surface mode:

$$\frac{P}{\Delta y} = 2\frac{\beta\gamma}{Z_0\chi}\left(\frac{mc^2\beta^3\gamma^3}{ek_0L^2}\right)^2 e^{2\Gamma_0 b}|\mathcal{E}|^2. \tag{35}$$

Since the power flows backward in the present case, the boundary condition for the field needs to be specified at the exit. In the TWA-type interaction, the power flows forward, and the boundary condition is specified at the entrance. This is an important difference between a TWA-type interaction and a BWO-type interaction. For our case, since we want to study the growth of signal from noise, we set $\mathcal{E}=0$ at $\zeta=1$. The noise comes from the random distribution of electrons in the longitudinal phase space.

The time-dependent analysis of BWO was first done by Ginzburg *et al.* [43], and later a more detailed analysis including the reflections at the ends was reported by Levush *et al.* [44]. In these anlayses, they consider the interaction of an annular beam with the slow wave supported by a corrugated waveguide. We converted their result for a case of the interaction of sheet beam with the surface mode supported by a grating and obtained an equation exactly the same as Eq. (21), as shown in Appendix A.

V. START-CURRENT CONDITION IN THE LINEAR REGIME

Before we proceed to the numerical solution of the nonlinear coupled Maxwell-Lorentz equations, we discuss the solution in the linear regime where the signal level is low. We discuss the growth rate (in time) of the signal and find the condition under which the real part of the growth rate is positive. In the BWO-type interaction, the real part of the growth rate is positive only if the beam current I is larger than the start current I_s. This means that the signal can build up in time only when the beam current is larger than the start current. This is known as the start oscillation condition and has been studied for BWO by Swegel [45]. Here, we perform a similar analysis for SP-FELs.

Let us start the analysis by assuming a perturbative eigensolution of Eqs. (31)–(34). For simplicity, we assume that the injected beam has monoenergetic distribution, and $\eta_i=0$ for all the electrons at $\zeta=0$. Further, we assume that the injected beam is unbunched, i.e., $\langle e^{-i\psi_0}\rangle=0$, where $\psi_{0,i}$ is the phase of the ith particle at $\zeta=0$. An equilibrium solution of the system of Eqs. (31)–(33) is obviously $\mathcal{E}=0$, $\eta_i=0$, and $\psi_i=\psi_{0,i}$. Let us define the perturbative solution by $\mathcal{E}=\tilde{\epsilon}$, $\eta_i=\delta\eta_i$, and $\psi_i=\psi_{0,i}+\delta\psi_i$. We introduce the following collective variables as done by Bonifacio *et al.* [46] for conventional FELs:

$$\tilde{x} = \langle\delta\psi e^{-i\psi_0}\rangle, \quad \tilde{y} = \langle\delta\eta e^{-i\psi_0}\rangle. \tag{36}$$

In terms of these variables, Eqs. (31)–(33) can be linearized and written as

$$\frac{\partial\tilde{\epsilon}}{\partial\tau} - \frac{\partial\tilde{\epsilon}}{\partial\zeta} = i\mathcal{J}\tilde{x}, \tag{37}$$

$$\frac{\partial\tilde{x}}{\partial\zeta} = \tilde{y}, \tag{38}$$

$$\frac{\partial\tilde{y}}{\partial\zeta} = \tilde{\epsilon} + Q\tilde{x}. \tag{39}$$

We assume the following form of the solution:

$$\tilde{\epsilon}(\zeta,\tau) = e^{\nu\tau}\Phi(\zeta), \quad \tilde{x}(\zeta,\tau) = e^{\nu\tau}\Psi(\zeta), \quad \tilde{y}(\zeta,\tau) = e^{\nu\tau}\Theta(\zeta). \tag{40}$$

Substituting the above solution into Eqs. (37)–(39), we obtain following equations:

$$\nu\Phi - \Phi' = i\mathcal{J}\Psi, \quad \Psi' = \Theta, \quad \Theta' = \Phi + Q\Psi, \tag{41}$$

where the $'$ denotes the derivative with respect to ζ. The above equation expresses Φ and Θ in terms of Ψ. The differential equation for Ψ is then written as

$$\Psi''' - \nu\Psi'' - Q\Psi' + \nu Q\Psi + i\mathcal{J}\Psi = 0. \quad (42)$$

Assuming a solution of the type $e^{\kappa\zeta}$ of the above third-order linear differential equation, we get the following algebraic equation for κ:

$$\kappa^3 - \nu\kappa^2 - Q\kappa + \nu Q + i\mathcal{J} = 0. \quad (43)$$

Note that ν is the growth rate in time, and κ is the the growth rate in space. The above equation is a cubic equation in κ, and it will have three solutions denoted by κ_1, κ_2, and κ_3, which will be functions of the growth rate ν, the dimensionless current $\mathcal{J}$, and the space-charge parameter Q. The general solution of Eq. (42) is then expressed as

$$\Psi = A_1 e^{\kappa_1\zeta} + A_2 e^{\kappa_2\zeta} + A_3 e^{\kappa_3\zeta}, \quad (44)$$

where A_1, A_2, and A_3 are constants to be determined by boundary conditions. The boundary conditions are (1) $\tilde{x}=0$ at $\zeta=0$ at all τ since the injected beam has no phase modulation, i.e., it is injected unbunched. This implies $\Psi=0$ at $\zeta=0$. (2) $\tilde{y}=0$ at $\zeta=0$ at all τ since the injected beam has no energy modulation, i.e., it is injected monoenergetically. This implies $\Psi'=0$ at $\zeta=0$. (3) $\tilde{\epsilon}=0$ at $\zeta=1$ for all τ since there is no external input at the end of the grating. This implies $\Psi'' - Q\Psi=0$ at $\zeta=1$. Combining these three boundary conditions, we find that a nontrivial solution exists only if the following condition is satisfied:

$$(\kappa_1^2 - Q)(\kappa_2 - \kappa_3)e^{\kappa_1} + (\kappa_2^2 - Q)(\kappa_3 - \kappa_1)e^{\kappa_2} + (\kappa_3^2 - Q)(\kappa_1 - \kappa_2)e^{\kappa_3} = 0. \quad (45)$$

For a given $\mathcal{J}$ and Q, the above equation is a transcendental equation in ν, and one can solve it numerically. For our parameters, Q is very small, and we take $Q=0$. For this case, we find that there exists a threshold value of $\mathcal{J}$ above which the real part of ν is positive. This threshold current is found to be 7.68. Our derivation here follows closely that of Swegle [45].

We can now write down an expression for the start current I_s, which needs to be exceeded in order that oscillations build up in an SP-FEL working as a BWO. The expression for I_s in terms of SP-FEL parameters can be written as

$$\frac{I_s}{\Delta y} = 7.685 I_A \frac{\beta^4\gamma^4\lambda}{2\pi^2\chi L^3} e^{2\Gamma_0 b}. \quad (46)$$

Putting $\beta=0.35$, $\gamma=1.07$, $\chi=10$ per cm, $\lambda=690$ μm, $L=12.7$ mm, and $b=10$ μm, we find the start surface current density to be 36.5 A/m. We would like to point out that Andrews *et al.* [47] have recently reported a calculation of the start current assuming an infinite electron beam along the x axis above the grating, treating the electron beam as a moving plasma dielectric. Following Swegle's analysis for a BWO, they obtain a start current of 1 mA, assuming a beam thickness of $\Delta y=20$ μm. This translates to a surface start current density of 50 A/m, which is slightly higher than our estimate of 36.5 A/m.

In our analysis, we chose $I/\Delta y=50$ A/m for which we find $\nu=0.62+i3.17$, using Eq. (45). The real part of ν gives us the growth rate in time. Converting to real variables, this gives us the e-folding time of the power in the surface mode to be 0.17 ns. The imaginary part of ν tells us how much the actual wavelength is detuned from the resonant wavelength. Again converting to real variables, this tells us that the power will actually build up at 694 μm rather than at the resonant wavelength of 690 μm.

VI. NUMERICAL SIMULATIONS

Since our equations and boundary conditions are similar to those obtained for BWO, we used the algorithm for simulating a BWO system developed by Ginzburg *et al.* [43] and later by Levush *et al.* [44]. Equations for electron dynamics [Eqs. (32) and (33)] for a given field distribution along the interaction region are solved by the predictor-corrector method. The space-charge field needed to solve the equation of motion is obtained from Eq. (34) for the known initial electron distribution in phase space. Knowing the modified electron distribution in phase space, the field distribution at the next time step is obtained by solving the partial differential equation [Eq. (31)] by the finite difference method. We have chosen the step size as $\Delta\tau=0.01$ and $\Delta\zeta=0.02$. As discussed in Ref. [43], the accuracy of this method is $O(\Delta\tau^2 + \Delta\zeta^2)$, and the method is stable for $\Delta\tau < \Delta\zeta$.

To initialize the electron beam in phase space, we use a quiet start scheme as well as the shot noise. In the quiet start scheme, if we have N particles, we set the intial phase of the nth particle to $2\pi n/N$. This ensures that initially $\langle e^{-i\psi}\rangle=0$. In this case, we initialize the initial field to a very small value to get started. At $\tau=0$, we set $\mathcal{E}=\delta\zeta^2$, where δ is a very small number. To simulate the shot noise, we have used the algorithm given by Penman and McNeil [48], which is commonly used in FEL codes. For the case of shot-noise initialization of the phase space, we set the initial field to zero.

We checked for the convergence of the solution by increasing the number of particles and reducing the step size. Based on this convergence test, we chose 1024 particles to be used in the simulation and used step sizes $\Delta\tau=0.01$ and $\Delta\zeta=0.02$. We also confirmed that the energy conservation is satisfied in the code at each integration step.

We have also performed the calculations taking the finite thickness of the electron beam along the x axis into account. This is done by assuming the beam to be composed of multiple layers, each layer being a sheet beam that can be treated the same way as discussed above. Further details of the equations are given in Appendix B.

We now discuss the results obtained using this code. Parameters used in the simulation are the same as discussed earlier in the paper. The grating length is taken to be 12.7 mm. First, we discuss the start current. For the BWO-type interaction, as discussed in the previous section, there is a threshold current that needs to be exceeded in order to achieve the power build-up starting from the noise. The solid curve in Fig. 7(a) shows the plot of start current versus the distance b of the sheet beam from the grating surface, as obtained from the numerical simulation. The dashed curve in the same figure is obtained analytically using Eq. (46). We find good agreement between the analytical calculation and the numerical simulation up to $b=40$ μm. For $b>40$ μm the growth rate in time is very low, and in the simulation we

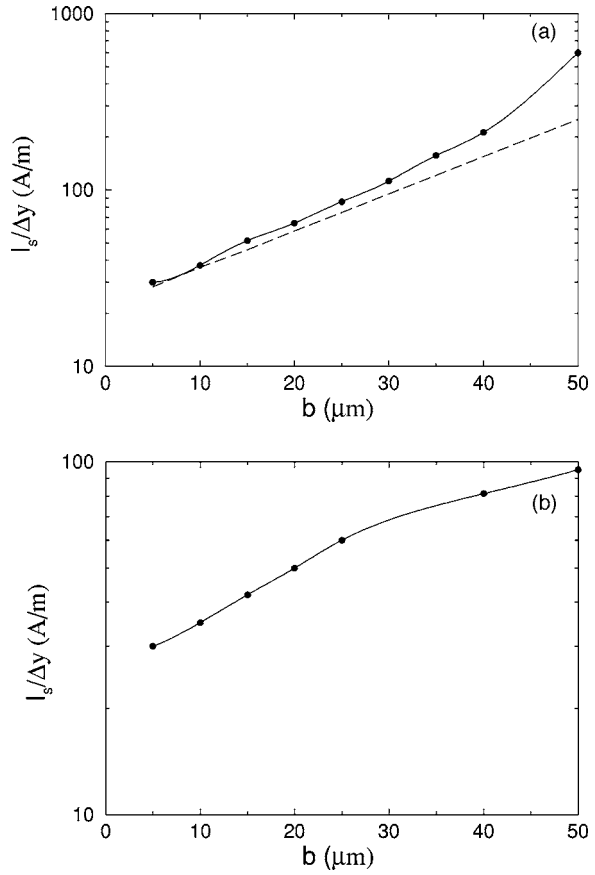

FIG. 7. Start-surface current density as a function of b for (a) a sheet electron beam at height b above the grating surface, and (b) a beam having thickness $2b$ and uniform distribution along the x axis. In the second case, the bottom of the beam touches the grating surface. In both cases, the electron beam is assumed to have infinite extent along the y axis. The solid curves in (a) and (b) are obtained from numerical simulation, whereas the dashed curve in (a) is obtained using an analytic formula [Eq. (46)].

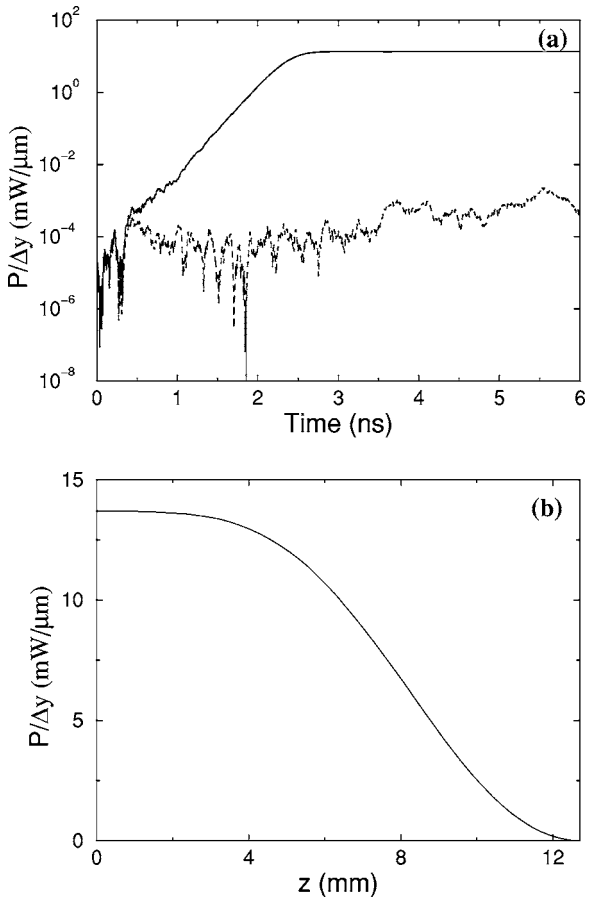

FIG. 8. Plots of power per unit beam width in the surface mode (a) as a function of time at $\zeta=0$, and (b) as a function of z at saturation as obtained from simulation. Parmeters used in the simulation are mentioned in Sec. V. Note that the solid curve in (a) is obtained for $I/\Delta y=50$ A/m, and the dashed curve is obtained for $I/\Delta y=36$ A/m, below the start current.

observe the exponential growth only if the beam current is sufficiently larger than the start current. The simulation therefore overestimates the start current. Figure 7(b) shows the same curve for a uniform density and finite-thickness beam instead of a sheet beam, taking the beam thickness to be $2b$ in the x direction and the bottom surface of the beam touching the top surface of the grating. Note that along the y direction we still assume that the beam has infinite extent. As seen in Fig. 7(b), we get a smaller start-surface current density compared to the sheet-beam case since a good part of the beam is sufficiently close to the grating.

For the sheet-beam simulation and taking $b=10$ μm, we find the start-surface current density to be 37.5 A/m, which agrees well with the analytic estimate of 36 A/m in the previous section. If we run the simulation for a surface current density less than 37.5 A/m, we only get a build up of extremely low-level noise. However, as shown in Fig. 8(a), for a surface current density of 50 A/m, the power per unit beam width builds up and saturates at 13.7 mW/μm. As shown in the same figure, for a surface current density of 36 A/m, we get random noise with a power level four to five orders of magnitude smaller. Also, we notice that for the 50-A/m case, the power builds up exponentially with time in the linear regime and the the power becomes e-folded in 0.20 ns, which agrees quite well with the estimate of 0.17 ns based on the analytic calculation in the previous section. We find that the power saturates in around 3 ns, which is around 15 times the e-folding time. The transit time for the electron beam through the grating is 120 ps. Hence, it takes 25 trips through the interaction regime for the power to saturate. This is similar to FEL oscillators, where it takes a few tens of round trips for the power to saturate. Figure 8(b) shows the growth of power along the interaction length after the system has reached saturation. We clearly see that power starts from zero at $\zeta=1$, i.e., at the end of the grating, then grows backward and reaches saturation at $\zeta=0$, i.e., at the begining of the grating. We also looked at the power spectrum and found that it is very narrow, consistent with a Fourier-transform-limited bandwidth. We found that the power is peaked at 694.5 μm, which means there is a detuning from the resonant wavelength. This detuning agrees quite well with the estimated detuning in the previous section based on analytic calculation.

When we keep increasing the surface current density, there is a second thresold at around 100 A/m after which the

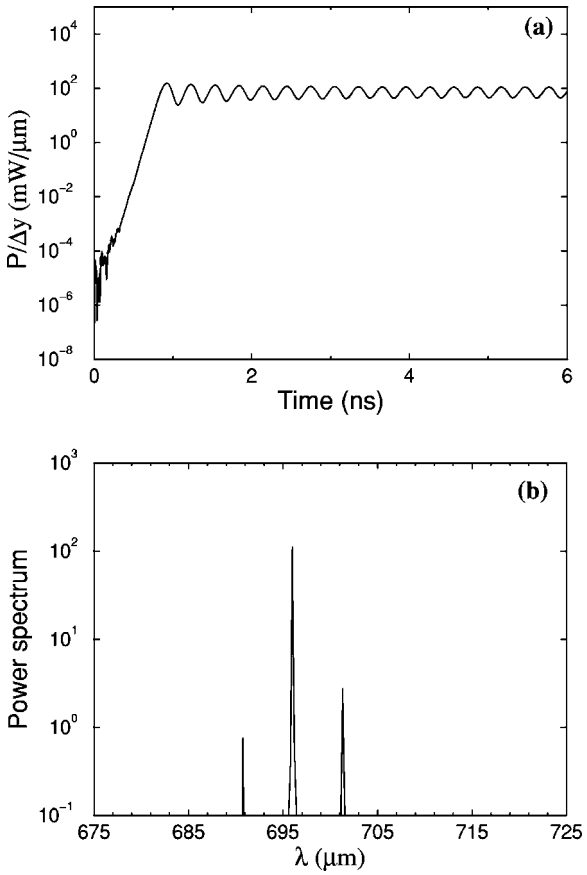

FIG. 9. Plots of power per unit beam width in the surface mode (a) as a function time for $I/\Delta y=120$ A/m. The modulation in the power is due to excitation at two nearby frequencies as seen in the power spectrum in (b).

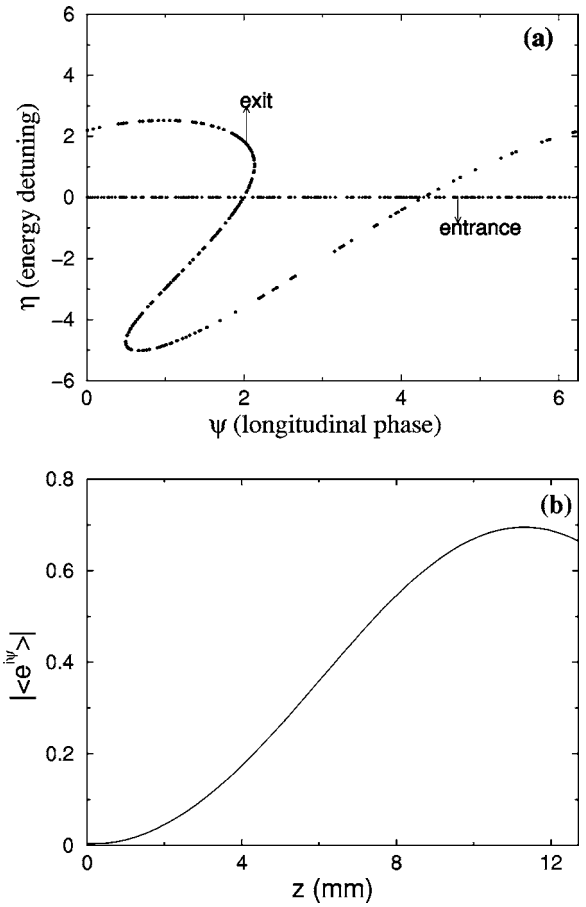

FIG. 10. The phase space (a) of the electron beam at the exit and at the entrance. Bunching is clearly seen. The growth of the bunching parameter along the interaction length is plotted in (b) after the power has saturated.

power is no longer stable at saturation and has modulations. Figure 9(a) shows such behavior for $I/\Delta y=120$ A/m. The corresponding power spectrum is shown in Fig. 9(b). We see that the power spectrum has peaks also at two nearby frequencies. The central peak is at 696 μm, and the two sidebands are at 691 μm and 701 μm, respectively. These sidebands can be understood to be due to synchrotron oscillations, as in the case of conventional FELs. An approximate expression for the synchrotron frequency for small-amplitude oscillation can be written using Eqs. (31)–(34), and one can derive the following expression for the wavelength shift $\Delta\lambda$ of the sidebands relative to the central frequency:

$$\Delta\lambda = \frac{\beta\lambda^2\sqrt{2|\mathcal{E}|}}{2\pi L}. \tag{47}$$

For the calculations in Fig. 9, $|\mathcal{E}|$ has modulation, but its mean value is 8.5, which can be substituted in the above equation and which gives us $\Delta\lambda=8.5$ μm. As we can see in Fig. 9(b), in our simulation we actually get $\Delta\lambda=5$ μm. This is in good agreement with our prediction keeping in mind that Eq. (47) is derived for small-amplitude motion in phase space. The transition from a single-frequency operation to a multifrequency operation is well known in the microwave BWO case [44], where the threshold for multifrequency operation was determined to be 2.4 times the start current. This seems to be valid approximately in our case, too.

We now look at the evolution of longitudinal phase space. Figure 10(a) shows the electrons' phase-space distributions when they enter and exit the interaction region. The phase-space distributions are plotted here after the power has saturated. We clearly see that the electrons become bunched due to the interaction with the surface mode. We plot the amplitude of the bunching parameter $|\langle e^{-i\psi}\rangle|$ along the interaction length after power has saturated in Fig. 10(b). We find that when the electrons exit the interaction region, they are nicely bunched and the bunching parameter is around 0.7. If the beam current is increased further, although more power is generated, the beam becomes overbunched as happens even in FELs.

We can now discuss the efficiency for power conversion in the SP-FEL system we are studying. For the 50-A/m case, the electron beam power per unit beam width is 1.75 W/μm, and the output optical power at the grating entrance is 13.7 mW/μm. Hence, the efficiency is $\sim$0.8%. For the 120-A/m case, the beam power per unit beam width is 4.2 W/μm, and the average output power is 81.2 mW/μm, which means the efficiency is 1.9%. The efficiency is higher

at this current, but power is not stable due to multifrequency excitation. We can get an analytic estimate for the upper bound of the efficiency by arguing that the maximum amount of energy that the electron can lose before saturation is such that it lags the copropagating evanescent wave by half a wavelength during the transit through the grating. If the change in the velocity of the electron due to loss of energy is Δv, then as per this argument, $\Delta v L/v = \pi v/\omega$, where $2\pi v/\omega$ is the wavelength of the zeroth-order evanescent wave. This gives us the following expression for the efficiency η_{eff}:

$$\eta_{eff} = \frac{1}{2}\frac{\lambda}{L}\frac{\beta^3\gamma^3}{(\gamma-1)}. \tag{48}$$

Using the above expression, we get an upper bound of 2% for the efficiency. This compares well with the observed value in the numerical simulation keeping in mind that this is only the estimate for the upper bound.

So far we have assumed that the electron beam has infinite extent along the y axis as does the radiation beam. Although we have not yet performed a rigorous three-dimensional (3D) analysis, we can estimate the 3D effects as follows. The radiation beam is guided by the grating along the x direction, but along the y direction the radiation beam will be freely diffracting. The minimum average rms beam size over the length L due to diffraction effects is given by $\sqrt{\beta\lambda L/4\pi}$ [49], which is around 500 μm for our parameters. Taking this as the effective electron beam radius in the y direction, $\Delta y = 1$ mm. Using this value of beam width, we obtain a start current of 37.5 mA. For $I = 50$ mA, the total power generated in the surface mode is then 13.7 W.

To summarize, we find that all the results of our numerical simulation show good agreement with the analytic calculation in the linear regime and also show the saturation behavior in the nonlinear regime. The efficiency at saturation is also in good agreement with the analytic estimate.

VII. OUTCOUPLING OF THE ELECTROMAGNETIC ENERGY

The results in the previous section indicate that, for our parameters, there will be a significant growth of power in the surface mode, and the electron beam becomes nicely bunched due to the interaction with the surface mode. The bunching wavelength will be the same as the spatial wavelength of the zeroth-order evanescent wave, i.e., $\beta\lambda$. Note that λ is the free-space wavelength of the evanescent wave. Hence, for our case, it turns out that the electron beam will become bunched at 241 μm. Also, the bunching will have components at higher harmonics. The power in the surface mode is in the form of near field. As we mentioned earlier, none of the spectral orders of this surface mode are radiative, and hence there is no far-field emission. In order to make it useful for experiments, it is important to be able to outcouple this electromagnetic energy in the form of freely propagating radiation. Here, we discuss some of the possible ways.

First, a good amount of energy stored in the surface mode will get outcoupled, via diffraction, to the freely propagating mode at the grating entrance. An exact calculation of the outcoupling efficiency due to diffraction that satisfies the boundary condition at the edge requires a lengthy calculation and will not be attempted here. We will, however, present some heuristic arguments. As explained in Sec. III, the surface mode mainly consists of an $n=1$ space harmonic, and the overall field profile is more like that of a freely propagating wave except that there is a small E_z component. We therefore expect that, like an incident freely propagating wave undergoing diffraction at the edge, a good fraction of the surface mode will be outcoupled. For the $n=1$ mode, the $1/e$ decay length, i.e., $1/\Gamma_1$, comes to be around 208 μm. Hence, the diffraction-limited divergence $\tan^{-1}(\lambda\Gamma_1/\pi)$ is estimated to be around 45°. Due to this large divergence, one can put a parabolic mirror near the grating entrance with a hole at the center sufficiently large to allow the electron beam to pass through. A significant portion of the outcoupled propagating wave will be incident outside the hole and will be reflected. If the mirror is tilted, the radiation incident on it can be directed to experiments. The outcoupling efficiency can be improved by designing a suitable matching end structure, for example, by slowly tapering the grating period at the entrance such that the $n=1$ space harmonic gradually becomes a freely propagating mode.

Second, one can make use of bunching at the harmonics. This has been earlier suggested by Andrews *et al.* [50]. If there is significant bunching at the harmonics, we could expect enhanced SP emission at higher harmonics of the fundamental free-space wavelength. For example, for our parameters there is expected to be enhanced SP emission at 345 μm, and this falls in the range of freely propagating SP radiation for our parameters. This radiation is expected to appear at an angle of 32° from the beam axis.

Third, we can make use of the bunching in the electron beam. When the electron beam exits, it is bunched, and a bunched beam undergoing transition from one medium (grating) to another medium (vacuum) is expected to give off coherent diffraction radiation at the transition. A rough estimate of the diffraction radiation can be obtained using a formula described by Potylitsyn for an electron passing above a metallic edge [51]. As per this model, when a train of electron bunches having charge q_b per bunch and bunch current I_b crosses a metallic edge at a perpendicular distance b from the bunch, the power in the diffraction radiation is given by

$$P_d = \frac{3}{4}\frac{I_b q_b \beta\gamma}{8\pi\epsilon_0 b}. \tag{49}$$

Putting the numbers in the above expression, we find that about 260 mW of radiation power can be generated in the form of diffraction radiation. Here, we have used the bunching parameter $\langle|e^{-i\psi_i}|\rangle = 0.6$. Hence, the bunch current $I_b = 0.6\times 50$ mA $= 30$ mA. The effective charge per bunch $q_b = \langle|e^{-i\psi_i}|\rangle I\lambda/c$ is about 0.069 pC, which has been used in the above formula.

Fourth, one can put a second grating after the first grating with suitably optimized parameters such that the free-space wavelength of the surface mode in the first grating falls in the range of freely propagating SP emission in the second grating. Let us illustrate this with an example. Let us choose

the grating parameters in the second grating to be $\lambda_{g2}=241.5\ \mu$m, $d_2=200\ \mu$m, and $a_2=150\ \mu$m. The electron beam enters the second grating bunched at wavelength λ_s. The beam current therefore can be expanded in Fourier series, and the current in the fundamental component can be written as

$$J_z(x,z,t)=\delta(x)\frac{I}{\Delta y}\langle e^{-i\psi}\rangle e^{i(\alpha_0 z-\omega_s t)}+\text{c.c.}, \tag{50}$$

where $\alpha_0=k_0$. As discussed in Sec. II, we can find out the incident field due to this and then, knowing the reflection matrix element, we can calculate the reflected field at all spectral orders. For this example, the $n=1$ spectral order will be propagating, and the magnetic field for this spectral order is given by

$$H_y^R(x,z,t)=-\frac{1}{2}e_{10}\frac{I}{\Delta y}\langle e^{-i\psi}\rangle e^{-(\Gamma_0-ip_1)b}e^{i(\alpha_1 z+p_1 x-\omega_s t)}+\text{c.c.} \tag{51}$$

Knowing the electromagnetic field, we can calculate the Poynting vector and then derive the following expression for the power radiated:

$$P=\frac{I^2 Z_0}{2\Delta y}|\langle e^{-i\psi}\rangle|^2 e^{-2\Gamma_0 b}|e_{10}|^2 L\sin\theta, \tag{52}$$

where θ is the angle at which the $n=1$ spectral order is radiated. For our parameters, $\sin\theta\approx 1$, $|e_{10}|^2$ is calculated to be 1.99, and $|\langle e^{-i\psi}\rangle|=0.6$. Putting all this in the above expression and using $\Delta y=1$ mm, we find that about 2.6 W of radiation power can be generated in this way for $I=50$ mA.

Hence, we find that it should be practically possible to outcouple a significant amount of coherent THz radiation power from a compact source based on a SP-FEL.

VIII. DISCUSSIONS AND CONCLUSIONS

Our analysis is built on earlier analyses by Van den berg [6–8], Kim and Song [14], and the BWO simulation reported in Refs. [43,44]. Van den berg's analysis is for evaluating spontaneous emission, and hence one looks at only those spectral orders that are radiative. For all these spectral orders, the reflection matrix element e_{m0} is finite as expected. In our calculation, since we have considered the stimulated emission, we looked at the amplitude of the zeroth-order reflected evanescent wave since the beam interacts resonantly with this wave. When we do that, we find that e_{00} becomes singular at a certain frequency, meaning that the grating supports a surface mode at this frequency. In order to proceed with the calculations while having this singularity in e_{00}, we realized that behavior around the singularity is conveniently described by the differential equation [Eq. (21)] rather than the algebraic equation [Eq. (7)].

In our analysis, we have looked at only the near-field term of the total electromagnetic field, and the near-field term is sharply peaked at a single frequency (690 μm in our case). In the far field, there will be spontaneous emission and enhanced spontaneous emission due to bunching of the electrons.

For the Dartmouth experiment, the radiation at 90° to the electron beam direction was examined. As per our calculation, at this wavelength the scattering matrix element does not have any significant dependence on the growth rate, and the quadratic equation for the growth rate obtained in Ref. [14] is valid. The growth rate for a wavelength corresponding to this is low, around 0.15 per cm, and hence not much SP radiation power is expected. Also, the operating beam current in the Dartmouth experiment [28] and even in the University of Chicago experiment [31] was much less than the start current for the BWO operation that we have calculated in this paper. Possibly, this is the reason why the 690 μm radiation escaping the ends of the grating that we have discussed in this paper has not been seen in any of these experiments.

In our analysis, we have considered the BWO-type interaction. As discussed earlier, for high-energy beam, the interaction could be of a TWA type. For those cases also, our analysis can be applied by changing the boundary conditions.

The earlier attempts to generate coherent SP radiation [9,10] were based on a resonator configuration. In our analysis, we do not have any resonator for positive feedback since the BWO-type interaction itself generates the positive feedback due to negative group velocity as noted by Andrews and Brau [15]. However, our approach can be attempted for performing the detailed simulation of the resonator-based schemes also.

In our simulation, we have not considered effects due to energy spread, emittance, and the effect of finite beam size. It is straightforward to add the energy spread to our simulation. In order to include the effect due to finite beam size and finite emittance, we need to do a 3D analysis, which we propose to do in the future. In general, the beam quality is a serious and limiting issue for the success of SP-FEL experiments.

Recently, Donohue and Gardelle have reported the numerical simulation of Smith-Purcell FELs using the particle-in-cell (PIC) approach [52]. The PIC simulations give more detailed information, but they are very time consuming. Our simulations based on Maxwell-Lorentz equations are much faster and hence can be more useful for performing detailed optimization studies.

Our analysis is general in nature in the sense that it can be applied to any grating profile. We have introduced a χ parameter, which characterizes the behavior of the grating for stimulated emission. One can evaluate the χ parameter of the grating by analyzing the singularity of e_{00} around the resonant wavelength. We would like to point out that for the conventional BWOs based on corrugated waveguides, Ginzburg *et al.* [43] and Levush *et al.* [44] have derived the Maxwell-Lorentz equations by taking the interaction of the electron beam with the copropagating surface mode into account. We have derived the coupled Maxwell-Lorentz equations for the SP-FEL case [Eqs. (31)–(34)] using this alternative approach also and we obtained exactly the same number for χ and χ_1 as we obtained using the residue approach described in this paper.

To summarize, we have presented a study of the SP-FEL dynamics by explicitly evaluating the reflection matrix elements for incident plane waves with slowly varying ampli-

tude. We have performed a numerical simulation of SP-FELs based on the BWO-type interaction. For our parameters, we find that around 14 W of electromagnetic power can be generated in the surface mode at 690 μm and the beam can be bunched at 241 μm due to this interaction. We have proposed that, in order to obtain copious emission at the bunching wavelength, the SP-FEL can be operated in two-grating mode with the first grating acting as the buncher and the second one acting as a radiator. Our analysis can be useful for the design of future SP-FEL experiments [49] and can be further extended to analyze the configuration using resonators.

APPENDIX A: ENERGY CONSERVATION

In this appendix, we derive the equation for the power in the backward wave using energy conservation. For simplicity, let us perform the calculation for steady state. Using Eqs. (31)–(34), we get

$$\frac{\partial|\mathcal{E}|^2}{\partial\zeta} = 2\mathcal{J}\,\mathrm{Re}[\mathcal{E}\langle e^{i\psi}\rangle], \tag{A1}$$

$$\frac{\partial\langle\eta\rangle}{\partial\zeta} = 2\,\mathrm{Re}[\mathcal{E}\langle e^{i\psi}\rangle] + 2\,\mathrm{Re}[\mathcal{E}_s\langle e^{i\psi}\rangle]. \tag{A2}$$

The second term on the right-hand side of Eq. (A2) can be shown to be zero using Eq. (34). Hence, combining the above two equations, we get

$$\frac{\partial}{\partial\zeta}[\mathcal{J}\langle\eta\rangle - |\mathcal{E}|^2] = 0, \tag{A3}$$

which is identified as the equation for conservation of energy. Note the negative sign of the second term within the square bracket, which is indicative of backward flow of energy. From this equation, we conclude that a change in the dimensionless beam energy $\langle\eta\rangle$ will result in the change in the field energy $|\mathcal{E}|^2$ of the backward wave as given by

$$\mathcal{J}[\langle\eta\rangle_{\zeta=0} - \langle\eta\rangle_{\zeta=1}] = |\mathcal{E}|^2_{\zeta=0} - |\mathcal{E}|^2_{\zeta=1}. \tag{A4}$$

In our case, $|\mathcal{E}|_{\zeta=1}=0$ and the energy lost by the beam in the interaction region appears in the field energy at the entrance in the backward wave. Using Eq. (27), we can obtain the expression for the energy lost by the beam per unit time in terms of $\langle\Delta\eta\rangle$ and that can be then expressed in terms of $|\mathcal{E}|^2$. From conservation of energy, this will be equal to the power in the backward wave. We obtain in this way the following expression for the power in the backward wave:

$$P = 2\frac{\beta\gamma\Delta y}{Z_0\chi}\left(\frac{mc^2\beta^3\gamma^3}{ek_0L^2}\right)^2 e^{2\Gamma_0 b}|\mathcal{E}|^2, \tag{A5}$$

which is Eq. (35).

Next, we will try to write down Eq. (21) in another familiar form. Knowing the above expression for P, we can write the expression for group velocity v_g in terms of $|E|^2$ and energy per unit length U by using $v_g = P/U$. Substituting this expression for v_g in the right-hand side of Eq. (16), we rewrite it as

$$\frac{\partial E}{\partial t} - v_g\frac{\partial E}{\partial z} = -\frac{I|E|^2}{U}\langle e^{-i\psi}\rangle, \tag{A6}$$

which is exactly the form obtained by Levush *et al.* [44] when transformed for our sheet-beam case. This justifies the arguments made while deriving Eq. (21).

APPENDIX B: MAXWELL-LORENTZ EQUATIONS FOR FINITE-THICKNESS BEAM

Here, we derive the equations used for simulating the finite-thickness beam. We assume that a finite-thickness beam can be described as a combination of N_l layers, where the lth layer is at a height $b_l = l\Delta x/N_l$ and carries a current I_l. The corresponding dimensionless current $\mathcal{J}_l$ is defined as

$$\mathcal{J}_l = 2\pi\frac{I_l}{I_A}\frac{\chi}{\Delta y}\frac{k_0L^3}{\beta^3\gamma^4}. \tag{B1}$$

The surface mode grows due to interaction with the current in all layers. The Maxwell equation for the evolution of the dimensionless amplitude of the surface mode is given by

$$\frac{\partial\mathcal{E}}{\partial\tau} - \frac{\partial\mathcal{E}}{\partial\zeta} = -\sum_{l=1}^{l=N_l}\mathcal{J}_l e^{-\Gamma_0 b_l}\langle e^{-i\psi}\rangle_l, \tag{B2}$$

where $\langle\ldots\rangle_l$ implies the averaging performed over the electrons in the lth layer. The equation of motion of the ith particle in the lth layer is given by

$$\frac{\partial\eta_i^l}{\partial\zeta} = (\mathcal{E}e^{-\Gamma_0 b_l} + \mathcal{E}_s^1 e^{-\Gamma_0 b_l} + \mathcal{E}_s^{2,l})e^{i\psi_i^l} + \text{c.c.}, \tag{B3}$$

$$\frac{\partial\psi_i^l}{\partial\zeta} = \eta_i^l, \tag{B4}$$

where $\mathcal{E}_s^1$ and $\mathcal{E}_s^{2,l}$ are given by

$$\mathcal{E}_s^1 = i\frac{\chi_1}{\chi L}\sum_{l'=1}^{l'=N_l}\mathcal{J}_{l'}e^{-\Gamma_0 b_{l'}}\langle e^{-i\psi}\rangle_{l'}, \tag{B5}$$

$$\mathcal{E}_s^{2,l} = -\frac{i}{\chi L}\sum_{l'=1}^{l'=N_l}\mathcal{J}_{l'}e^{-\Gamma_0|b_l - b_{l'}|}\langle e^{-i\psi}\rangle_{l'}. \tag{B6}$$

Finally, the power flowing in the backward direction in the surface mode is given here by

$$\frac{P}{\Delta y} = 2\frac{\beta\gamma}{Z_0\chi}\left(\frac{mc^2\beta^3\gamma^3}{ek_0L^2}\right)^2|\mathcal{E}|^2. \tag{B7}$$

Note that the surface current density can be different in different layers, and hence one can simulate any arbitrary beam profile along the x axis. We however do not take into account any force acting on the beam in the x direction, and therefore the transverse beam profile remains the same everywhere in the interaction regime. This is an approximation used in our analysis.

[1] I. M. Frank, Izv. Akad. Nauk SSSR, Ser. Fiz. **6**, 3 (1942).
[2] W. Salisbury, U.S. Patent No. 2634372 (1949).
[3] S. J. Smith and E. M. Purcell, Phys. Rev. **92**, 1069 (1953).
[4] G. Toraldo di Francia, Nuovo Cimento **16**, 61 (1960).
[5] K. Ishiguro and T. Tako, Opt. Acta **8**, 25 (1961).
[6] P. M. Van den berg, J. Opt. Soc. Am. **63**, 689 (1973).
[7] P. M. Van den berg, J. Opt. Soc. Am. **63**, 1588 (1973).
[8] P. M. Van den berg and T. H. Tan, J. Opt. Soc. Am. **64**, 325 (1974).
[9] J. M. Wachtel, J. Appl. Phys. **50**, 49 (1979).
[10] L. Schachter and A. Ron, Phys. Rev. A **40**, 876 (1989).
[11] O. Haeberle, P. Rullhusen, J. M. Salome, and N. Maene, Phys. Rev. E **49**, 3340 (1994).
[12] J. Walsh, K. Woods and S. Yeager, Nucl. Instrum. Methods Phys. Res. A **341**, 277 (1994).
[13] J. H. Brownell, J. Walsh, and G. Doucas, Phys. Rev. E **57**, 1075 (1998).
[14] K.-J. Kim and S. B. Song, Nucl. Instrum. Methods Phys. Res. A **475**, 158 (2001).
[15] H. L. Andrews and C. A. Brau, Phys. Rev. ST Accel. Beams **7**, 070701 (2004).
[16] F. S. Rusin and G. D. Bogmolov, Proc. IEEE **57**, 720 (1969).
[17] W. W. Salisbury, J. Opt. Soc. Am. **60**, 1279 (1970).
[18] J. P. Bachheimer, Phys. Rev. B **6**, 2985 (1972).
[19] K. Mizuno, S. Ono, and Y. Shibata, IEEE Trans. Electron Devices, **20**, 749 (1973).
[20] E. L. Burdette and G. Hughes, Phys. Rev. A **14**, 1766 (1976).
[21] R. P. Leavitt, D. E. Wortman, and H. Dropkin, IEEE J. Quantum Electron. **17**, 1333 (1981).
[22] D. E. Wortman, H. Dropkin, and R. P. Leavitt, IEEE J. Quantum Electron. **17**, 1341 (1981).
[23] A. Gover, P. Dvorkis, and U. Elisha, J. Opt. Soc. Am. B **1**, 723 (1984).
[24] I. Shih *et al.*, Opt. Lett. **15**, 559 (1990).
[25] G. Doucas, J. H. Mulvey, M. Omori, J. Walsh, and M. F. Kimmitt, Phys. Rev. Lett. **69**, 1761 (1992).
[26] K. J. Woods, J. E. Walsh, R. E. Stoner, H. G. Kirk, and R. C. Fernow, Phys. Rev. Lett. **74**, 3808 (1995).
[27] K. Ishi, Y. Shibata, T. Takahashi, S. Hasebe, M. Izekawa, K. Takami, T. Matsuyama, K. Kolayashi, and Y. Fujita, Phys. Rev. E **51**, R5212 (1995).
[28] J. Urata, M. Goldstein, M. F. Kimmitt, A. Naumov, C. Platt, and J. E. Walsh, Phys. Rev. Lett. **80**, 516 (1998).
[29] A. Doria *et al.*, Nucl. Instrum. Methods Phys. Res. A **475**, 318 (2002).
[30] G. Kube *et al.*, Phys. Rev. E **65**, 056501 (2002).
[31] O. H. Kapp, Y.-e Sun, K.-J. Kim, and A. V. Crewe, Rev. Sci. Instrum. **75**, 4732 (2004).
[32] S. E. Korbly, A. S. Kesar, J. R. Sirigiri, and R. J. Temkin, Phys. Rev. Lett. **94**, 054803 (2005).
[33] Lord Rayleigh (J. W. Strutt), Proc. R. Soc. London, Ser. A **79**, 399 (1907).
[34] *Electromagnetic Theory of Gratings*, edited by R. Petit (Springer-Verlag, Berlin, 1980).
[35] K.-J. Kim, Nucl. Instrum. Methods Phys. Res. A **250**, 396 (1986).
[36] P. M. Van den berg, Appl. Sci. Res. **24**, 261 (1971).
[37] F. J. Crowne, R. P. Leavitt, and T. L. Worchesky, Phys. Rev. A **24**, 1154 (1981).
[38] B. Hafizi, P. Sprangle, and P. Serafim, Phys. Rev. A **45**, 8846 (1992).
[39] V. Kumar and K.-J. Kim, presented at PAC05.
[40] M. Neviere, in *Electromagnetic Theory of Gratings*, edited by R. Petit (Springer-Verlag, Berlin, 1980).
[41] H. R. Johnson, Proc. IRE **34**, 684 (1955).
[42] W. B. Colson, Phys. Lett. **59A**, 187 (1976).
[43] N. S. Ginzburg, S. P. Kuznetzov, and T. N. Fedoseeva, Sov. Radiophys., **21**, 728 (1979).
[44] B. Levush *et al.*, IEEE Trans. Plasma Sci. **20**, 263 (1992).
[45] J. A. Swegle, Phys. Fluids **30**, 1201 (1987).
[46] R. Bonifacio, C. Pelligrini, and L. M. Narducci, Opt. Commun. **40**, 373 (1984).
[47] H. L. Andrews, C. H. Boulware, C. A. Brau, and J. D. Jarvis, Phys. Rev. ST Accel. Beams **8**, 050703 (2005).
[48] C. Penman and B. W. J. McNeil, Opt. Commun. **90**, 82 (1992).
[49] K.-J. Kim, V. Kumar, O. H. Kapp, and A. V. Crewe (unpublished).
[50] H. L. Andrews, C. H. Boulware, C. A. Brau, and J. D. Jarvis (private communication).
[51] A. P. Potylitsyn, Nucl. Instrum. Methods Phys. Res. B **145**, 169 (1998).
[52] J. T. Donohue and J. Gardelle, Phys. Rev. ST Accel. Beams **8**, 060702 (2005).